



Temperature dependent crossover between positive and negative magnetoresistance in graphene nanocrystallines embedded carbon film

Dong Ding, Xingze Dai, Chao Wang*, Dongfeng Diao

Institute of Nanosurface Science and Engineering, Guangdong Provincial Key Laboratory of Micro/Nano Optomechatronics Engineering, College of Mechatronics and Control Engineering, Shenzhen University, Shenzhen, 518060, China

ARTICLE INFO

Article history:

Received 31 January 2020

Received in revised form

2 March 2020

Accepted 9 March 2020

Available online 10 March 2020

ABSTRACT

Monitoring magnetoelectric transport behavior of graphene material is critical in establishing a foundation for engineering next-generation spintronic devices. Here we report a temperature-dependent crossover between positive and negative magnetoresistance (MR) in graphene nanocrystallines embedded carbon film (GNC film), two sign changes of MR_{Total} (where MR_{Total} presents the measured MR value) value from positive $MR_{Total}(+)$ to negative $MR_{Total}(-)$ and then back to $MR_{Total}(+)$ are observed as temperature varies from 2 K to 400 K. The crossover can be ascribed to the competitions among different origins including wave function shrinkage, spin-dependent Coulomb blockade effect and Lorentz force, which play dominant roles in low, medium and high temperatures, respectively. Moreover, it is revealed that GNC film with smaller GNs has larger positive contribution to MR_{Total} behavior, resulting in maximum $MR_{Total}(+)$ of $\sim 8.1\%$. In contrast, GNC film with larger GNs dramatically contributes to negative MR_{Total} behavior, which obtains maximum $MR_{Total}(-)$ of $\sim -1.1\%$. This work deepens understanding about the origin of MR of nanometer-sized graphene, which provides guidance for further magnetoelectric property improvement, and paves a way towards specific design of graphene derived spintronic devices with controllable MR behavior.

© 2020 Elsevier Ltd. All rights reserved.

1. Introduction

Magnetoresistive effect is of great interest in spintronics and microelectronic applications, such as magnetic sensors, magnetic random access memory, spin logic and biomolecular diagnostics [1–5]. Combining the advantages of low weight, low spin-orbit coupling, high thermal conductivity and nontoxicity, graphene opens a suitable window for applications in magnetoresistance (MR) devices [6–11]. MR behaviors of various kinds of graphene-based materials were studied in recent years [12–14]. Zhi-Min Liao et al. observed large positive MR effect from few layered graphene stacks, and MR value was anisotropic which relied on the direction of external magnetic field [15]. The MR effect of graphene-based material was considered to arise from edge states, which was regarded as main sources of the intervalley scattering thus causing

restoration of weak localization (WL) [16,17]. It was confirmed by many works that introducing more edge states of graphene, such as creating zig-zag edges and defects, can result in occurrence of prominent MR behavior [18,19]. Nanometer-sized graphene obtained more localized unpaired spins arising from bonding defects at edge state, has shown great development prospects for large MR [20]. Moreover, due to the synergistic effect of quantum confinement and rich heterogeneous interfaces in nanometer-sized graphene, transport properties of electrons and magnetic properties will be significantly modulated [21–23]. Recently, Raghav Garg et al. observed negative MR magnitudes on order of 1%–4% at low temperature from 3D fuzzy graphene nanostructure. Their work extended studies about the MR behavior into multidimensional graphene nanostructures [24]. Controllable transition between negative and positive MR behavior from one material, which can be driven by carrier type, voltage, and magnetic field, is a crucial character for its application in spintronic devices [25–27]. Investigations on the transition of MR behavior can deepen the understanding of its origin, which is of great concern for further MR property improvements and applications.

* Corresponding author.

E-mail addresses: ddinju@hotmail.com (D. Ding), 1800291007@email.szu.edu.cn (X. Dai), cwang367@szu.edu.cn (C. Wang), dfdiao@szu.edu.cn (D. Diao).

Herein, we observed temperature driven transition from positive to negative MR behavior in vertical graphene nanocrystallines embedded carbon film (denoted as GNC film). That is, in low temperature, the MR_{Total} values (where MR_{Total} presents the measured MR value) of GNC film are positive and present saturation trend in high magnetic field, which is proposed to arise from the shrinkage of orbits (wave functions of electrons). With the temperature increasing, positive MR_{Total} (denoted as $MR_{Total}(+)$) gradually decreases and then transforms into negative MR_{Total} (denoted as $MR_{Total}(-)$). The negative MR is proposed to be generated by the effect of spin-dependent Coulomb blockade, which is generated by the enhanced electrons tunneling probability between graphene nanocrystallines (GNs) and the decreased resistance. The second transition from negative to positive MR_{Total} behavior appears with temperature further increases, the positive MR_{Total} is unsaturated and linearly increased with B. This is indicative of that the origin of positive MR in this temperature range can be regarded as effect of Lorentz force. Furthermore, we regulated the size of GNs in GNC film, and we systematically investigated its influence on MR behavior. This work brings forth a significant progress in comprehending of physics of carbon material, it also extends the employment of GNs into spintronics with tailor-able MR behavior.

2. Experimental and measurement details

2.1. Synthesis of GNC film

The GNC film was synthesized using ECR plasma sputtering system (as schematic diagram shows in Fig. s1 in SI). In brief, GNC film was deposited on silicon substrate by low energy electron irradiation technique, argon plasma was introduced during GNC film deposition. The size of GNs in GNC film was controlled by adjusting electron irradiation energy ranging from 40 eV to 100 eV. Pure amorphous carbon film was synthesized under 0 eV.

2.2. Sample characterization

The morphology of GNC films were measured using a JEOL-2010 TEM with the electron acceleration voltage of 200 kV. Raman spectra were collected by HORIBA HR800 laser confocal Raman spectrometer, by using 514 nm laser (0.1 mW) with a spot of 2 μ m. Magnetoresistance characterizations were carried on by a Physical Property Measurement System (PPMS DynaCool, Quantum Design) using four-probe-method, in the temperature ranging from 2 K to 400 K and magnetic field with the strength range of ± 9 T. The magnetic field was applied perpendicular to GNC film. Magnetic properties were collected by PPMS in a temperature range from 10 K to 400 K, the diamagnetic contribution of the substrate has been subtracted from all the data.

3. Results and discussion

The films were deposited on silicon substrate by low energy electron irradiation technique (the schematic diagram of the system is shown in Fig. s1). We varied the electron irradiating energies (ranging from 0 eV to 100 eV) during film deposition. The morphologies of as deposited films were measured by high-resolution transmission electron microscopy (HR-TEM), as shown in Fig. 1. HR-TEM image of film deposited at 0 eV shows a uniform amorphous morphology. Some nanocrystallines are observed from the film deposited at 40 eV, which are embedded in the amorphous matrix. The lattice spacing of nanocrystalline is about 0.38 nm, which matches well with the inter-planar distance of (002) graphite, indicating that nanocrystallines are composed of few-

layer graphene [28]. Moreover, the average size of the graphene nanocrystallines (GNs) increase as the electron irradiating energy enhances. The insets in Fig. 1 (b)–(e) present the size distribution of GNs in the film, wherein the average size (R_{avg}) of GNs are about 3.7 nm (40 eV), 5.5 nm (60 eV), 6.7 nm (80 eV) and 10.5 nm (100 eV), these samples are denoted as GNC-3.7 nm, GNC-5.5 nm, GNC-6.7 nm and GNC-10.5 nm, respectively. Thickness of the film is around 70 nm, as shown in Fig. s2. The enlarged side view image in Fig. 1 (f) shows that GNs are vertically aligned on the Si substrate.

Fig. 2 shows Raman spectra of films prepared with different electron irradiation energies. Raman spectrum of film prepared at irradiation energy of 0 eV exhibits broad band from 1200 to 1800 cm^{-1} , furthermore, characteristic peak of 2D mode at round 2700 cm^{-1} is not observed, confirming the absence of graphene in this film. When the electron irradiation energy increases up to 40 eV, typical D peak, G peak and 2D peak are observed at wavelengths of 1347 cm^{-1} , 1600 cm^{-1} and 2680 cm^{-1} , respectively. The observed strong D peak in Raman spectrum reveals the defects in GNC film, which are generated by the rich edge states of GNs [29]. As shown in Fig. 2 (b), intensity ratio of G and D modes I_D/I_G gradually increases for GNC film prepared under higher irradiation energy (detailed fitting results are shown in Fig. s3), indicating the existence of more graphene edges in GNC film [30]. These results are in accordance with the HR-TEM images.

Temperature dependence of the resistivity ($\rho - T$) for GNC films and amorphous carbon film are measured using four-probe-method as schematic diagram shows in Fig. s4 (a). The $\rho - T$ curves of GNC-3.7 nm, GNC-5.5 nm, GNC-6.7 nm and GNC-10.5 nm samples are given in Fig. 3 (a)–(d), and the $\rho - T$ curve of amorphous carbon film is shown in Fig. s4 (b). Decreases in resistivity with increasing temperature in the absence of magnetic field and 9 T are observed for all samples. Moreover, as represented in insets of Fig. 3 and Fig. s5, $\ln(\rho)$ dates of all GNC films with different GN sizes are more in accordance with $T^{-1/4}$ in the 2–150 K temperature range, claiming MOTT-VRH conduction. Nevertheless, for each GNC film, when the temperature increases from 2–50 K to 50–150 K, it is observed that R-square values of linear fitting results from $\ln(\rho)$ vs. $T^{-1/4}$ (MOTT-VRH) shows decrease tendency, whereas R-square from $\ln(\rho)$ vs. $T^{-1/2}$ (ES-VRH) shows increase tendency. This phenomenon point to the trend of Coulomb interaction with temperature increases within the temperature range from 50 to 150 K. According to Mott's VRH theory, low temperature electron transport occurs via tunnel hopping near the Fermi level between the localized states in GNC films [31,32]. As a comparison, the transport properties of pure carbon film was investigated by plotting $\ln(\rho)$ vs. $T^{-1/4}$ and $T^{-1/2}$, as shown in Fig. s6. The curve for pure carbon film fit very well with $T^{-1/2}$ behavior, rather than that with $T^{-1/4}$, indicating that pure amorphous carbon film is more in accordance with ES-VRH conduction. These results demonstrate that the transport properties of carbon film are dramatically changed by introducing GNs.

MR as a function of magnetic field strength (from -9 T to 9 T) at different temperatures for GNC films and bare amorphous carbon film are investigated. Herein, MR is defined as:

$$MR = \frac{\rho(B) - \rho(0)}{\rho(0)} \quad (1)$$

where B is the applied magnetic field, $\rho(0)$ and $\rho(B)$ are resistivities of film in the presence and absence of magnetic field, respectively [33].

Fig. 4 and Fig. 6 (a) present MR_{Total} value as a function of temperature and magnetic field of GNC films. It is observed that with the temperature increases, MR_{Total} values of GNC film samples are characterized with gradual transition from positive to negative (the

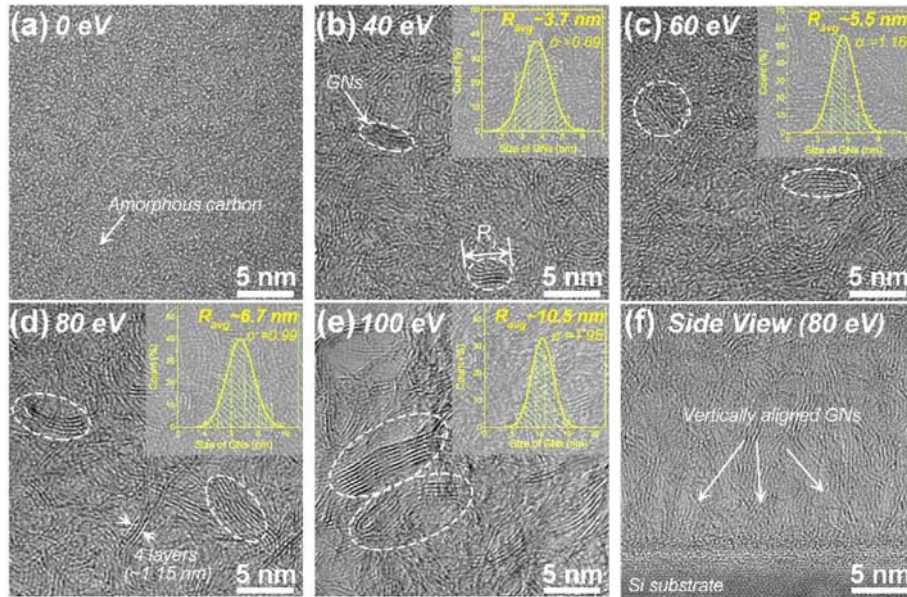


Fig. 1. High-resolution transmission electron microscopy (HR-TEM) images from the top view of GNC film prepared at different electron irradiating energies (a) 0 eV; (b) 40 eV; (c) 60 eV; (d) 80 eV; (e) 100 eV; the insets are measured size distribution histogram of GNs in each film; (f) enlarged side view of HR-TEM image at the interface of GNC film and Si substrate. (A colour version of this figure can be viewed online.)

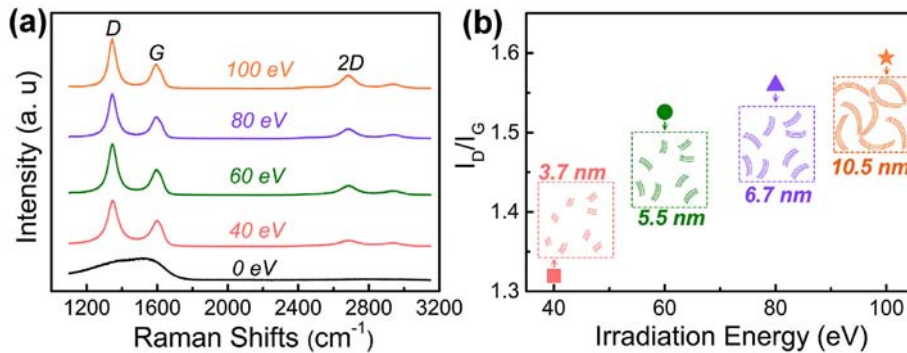


Fig. 2. (a) Raman spectra; (b) intensity ratio of G and D modes I_D/I_G of films prepared by low energy electron irradiation technique with different electron irradiation energy ranging from 0 eV to 100 eV. (A colour version of this figure can be viewed online.)

first transition), then MR_{Total} values switch from negative to positive (the second transition) as temperature further increases. However, these two thermal driven transitions of MR_{Total} values are not observed in pure amorphous carbon film (as shown in Fig. S7), indicating the transitions of MR_{Total} behavior are attributed to GNs. At 2 K and 9 T, MR_{Total} (+) values of GNC-3.7 nm, GNC-5.5 nm, GNC-6.7 nm and GNC-10.5 nm are around 8.1%, 3.8%, 3.5% and 2.3%, respectively. These results indicate that the film with smaller GNs has larger MR_{Total} (+).

MR_{Total} behavior can be regarded as a sum of contributions of wave function shrinkage effect (MR_{WFS} (+)), spin-dependent Coulomb blockade effect (MR_{SDCB} (-)) and Lorentz force (MR_{LF} (+)), each of which play dominant roles in low, medium and high temperature ranges, respectively, as following:

$$MR_{Total} = MR_{WFS} (+) + MR_{SDCB} (-) + MR_{LF} (+) \quad (2)$$

Low-temperature positive MR may arise from the wave function shrinkage in a perpendicular magnetic field (MR_{WFS} (+)). Above ρ - T curves describe that low-temperature (ranging from 2 K to 50 K) conductivity of GNC film samples follow the Mott-VRH model,

which features as overlapped wave functions with each other of the localized electronic states. MR_{WFS} (+) is a consequence of fact that applying a magnetic field will contract wave functions of electrons and reduce the overlap states, consequently decrease the electron hopping probability between these two states. Typically, in this situation, $\rho(0)$ and $\rho(B)$ follow the relationship below [34,35]:

In weak magnetic field (below characteristic field):

$$\ln \frac{\rho(B)}{\rho(0)} \propto B^2 \cdot T^{-\frac{3}{4}} \quad (3)$$

In strong magnetic field (above characteristic field):

$$\ln \frac{\rho(B)}{\rho(0)} \propto B^{\frac{1}{2}} \cdot T^{-\frac{1}{3}} \quad (4)$$

where B is the magnetic field, T is the temperature. Fig. 4 (a₂)-(d₂) show the plot of $\ln(\rho(B)/\rho(0))$ vs. B^2 of GNC films at 2 K. The $\ln(\rho(B)/\rho(0))$ values of GNC films linearly increase with B^2 up to their characteristic field (MR tends to be saturated in magnetic field above the characteristic field). Moreover, with the increasing size of

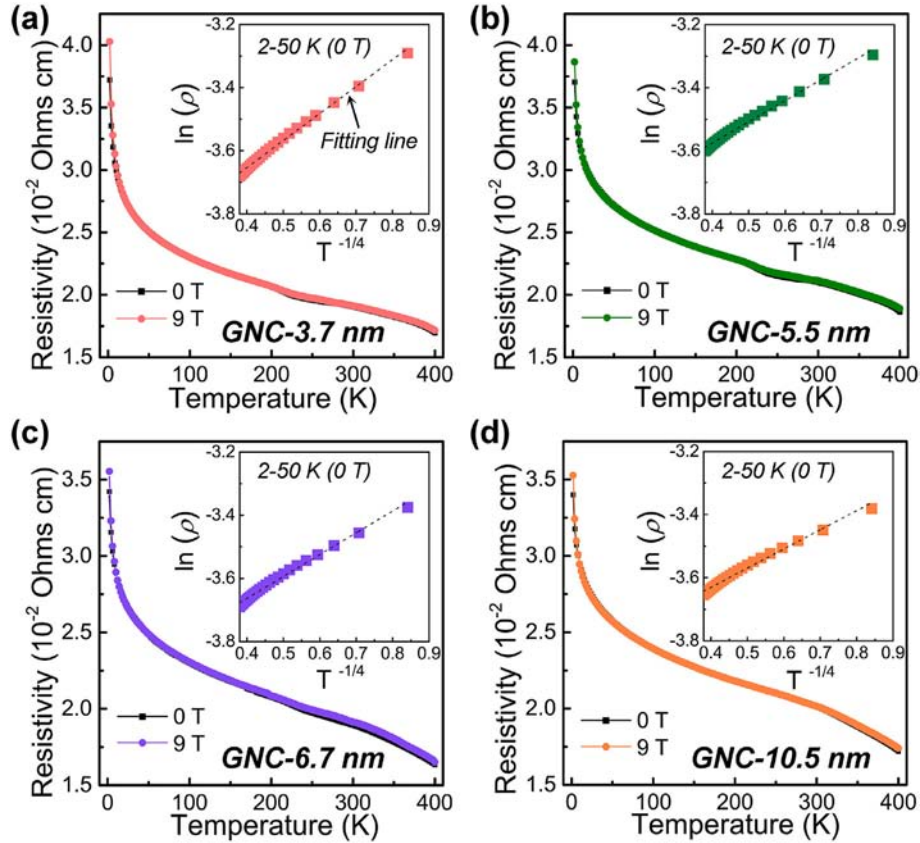


Fig. 3. Resistivity as a function of temperature for (a) GNC-3.7 nm; (b) GNC-5.5 nm; (c) GNC-6.7 nm; (d) GNC-10.5 nm films. The insets represent conductivity plotted as $\ln(\rho)$ vs. $T^{-1/4}$. Dashed lines are the best linearity fitting results. (A colour version of this figure can be viewed online.)

GNCs in GNC-3.7 nm, GNC-5.5 nm, GNC-6.7 nm and GNC-10.5 nm, $MR_{\text{Total}} (+)$ decreases from 8.1% to 2.3%, which is due to the enlarged overlapped wave functions of localized electronic states in GNCs. As shown in Fig. 4 (a₃)-(d₃), the linearity between $\ln(\rho(B)/\rho(0))$ values and $B^{1/3}$ exists in magnetic field above characteristic field. These results are qualitative in agreement with the wave function shrinkage theory. Another positive contribution to MR_{Total} at 2 K may be the spin effects in strongly localized systems. As can be observed from Fig. 4, MR values of our samples present linear dependence at lower magnetic fields and show trend of saturation as magnetic field increases. According to Kurobe and Kaminura's results [36], in consideration of Coulomb repulsion, states at the Fermi level may be singly occupied, doubly occupied or unoccupied. Spins will be aligned by external magnetic field, which causes in more difficult hopping between these states due to spin exchange and results in positive MR. In high magnetic field, all of the spins are aligned and MR behavior tends to be saturated.

As shown in Figs. 4 and 6 (a), a transition from $MR_{\text{Total}} (+)$ to $MR_{\text{Total}} (-)$ appears when temperature reaches ~27 K (GNC-3.7 nm), ~10 K (GNC-5.5 nm), ~9 K (GNC-6.7 nm) and ~6 K (GNC-10.5 nm). The contribution of $MR (-)$ becomes more pronounced as temperature rises, until up to the second transition temperature.

We propose the spin-dependent Coulomb blockade effect as a feasible mechanism for producing negative MR ($MR_{\text{SDCB}} (-)$). As temperature increases, the thermally activated electrons tunneling induced conductance is realized near the Fermi level (VRH) between the localized states [37]. We explored the magnetic properties of GNC film and the results are shown in Fig. 5. Fig. 5 (a) shows the magnetic properties of GNC film collected at various temperatures, indicating that the GNC film exhibits ferromagnetic

hysteresis behavior in the temperatures ranging from 10 K to 400 K. Moreover, as shown in Fig. 5 (b), we note that ferromagnetic moment of the GNC film decreases as temperature increases, suggesting a suppression of magnetic order by thermal disturbance. Owing to the spin-dependent Coulomb blockade effect, resistivity of GNC film decreases with lower scattering rate of the conducting electrons dominated by magnetic moment orientation varied from random to order in a magnetic field [38–40].

Moreover, as clearly shown in Fig. 6 (a), GNC film with larger GNCs has larger MR (-), leading to lower first transition temperature and higher second transition temperature. As the average size of GNCs increases according to the enhancement of electron irradiation energy, their average distance between GNCs barely changes (see Fig. s8). Therefore, larger MR (-) can be considered as the consequence of higher hopping probability between larger GNCs. The potential of GN increases ΔE when it gains each of electrons, hopping conduction electrons will have to surmount the potential barrier to enter the GN. Thus, electron tunneling probability is affected by the potential barrier. ΔE is inversely proportional to the size of GN as the relationship below [41]:

$$\Delta E = \frac{e^2}{2\pi\epsilon_0\epsilon R} \quad (5)$$

where e is the elementary charge, ϵ and ϵ_0 are the values of permittivity of vacuum and the dielectric constant of the material, R is the size of nanocrystalline. ΔE of GNC film with larger GNCs is smaller, resulting in higher electron tunneling probability and more prominent $MR_{\text{SDCB}} (-)$, as schematic diagram shows in Fig. 6 (b). Nevertheless, as evidenced by above magnetic measurement

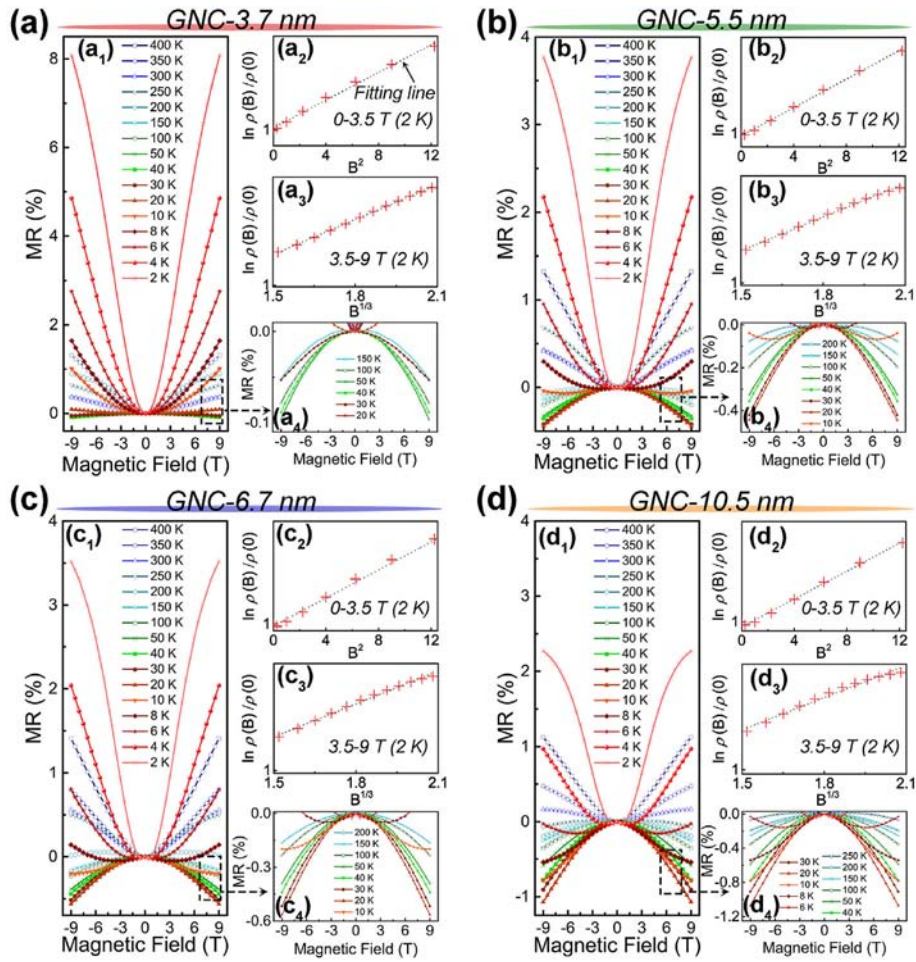


Fig. 4. MR as a function of magnetic field strength (from -9 T to 9 T) at different temperatures for (a₁) GNC-3.7 nm; (b₁) GNC-5.5 nm; (c₁) GNC-6.7 nm; (d₁) GNC-10.5 nm films, the enlarged negative MR plots are shown in the bottom right of (a₄)-(d₄). $\ln \rho(B)/\rho(0)$ vs. B^2 (in magnetic field ranging from 0 to 3.5 T, at 2 K), $\ln \rho(B)/\rho(0)$ vs. $B^{1/3}$ (in magnetic field ranging from 3.5 to 9 T, at 2 K) and fit results (dashed lines) for (a₂), (a₃) GNC-3.7 nm; (b₂), (b₃) GNC-5.5 nm; (c₂), (c₃) GNC-6.7 nm; (d₂), (d₃) GNC-10.5 nm films. (A colour version of this figure can be viewed online.)

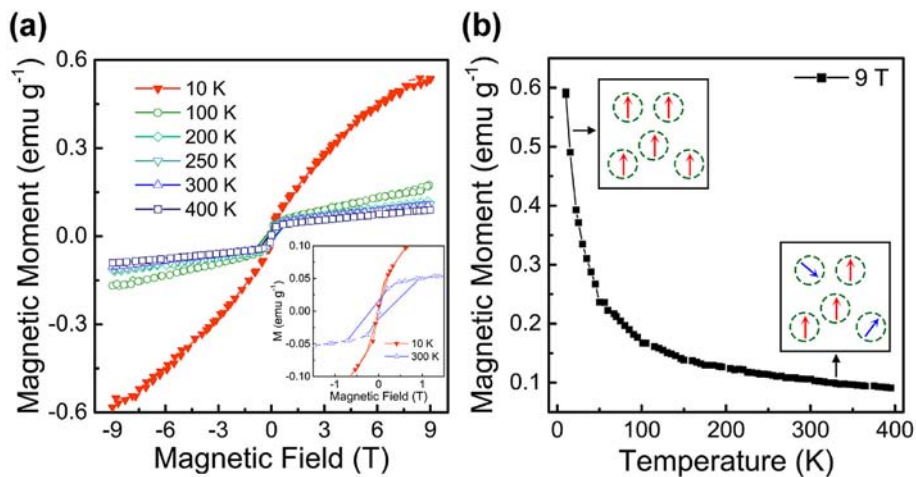


Fig. 5. (a) Magnetization vs. magnetic field ($M - H$) of GNC film at 10 – 400 K, the inset is enlarged $M - H$ curves collected at 10 K and 300 K; (b) Magnetization vs. T measured at 9 T. The diamagnetic contribution of the substrate has been subtracted from all the data. (A colour version of this figure can be viewed online.)

results that magnetic order decreases as temperature increases, where the decrease of spin-dependent electron tunneling is indistinctive and the donation of MR_{SDCB} ($-$) becomes feeble, this is

also the reason why transition from MR_{Total} ($-$) to MR_{Total} ($+$) behavior appears as the temperature further increases.

The following transition from MR_{Total} ($-$) into MR_{Total} ($+$) occurs

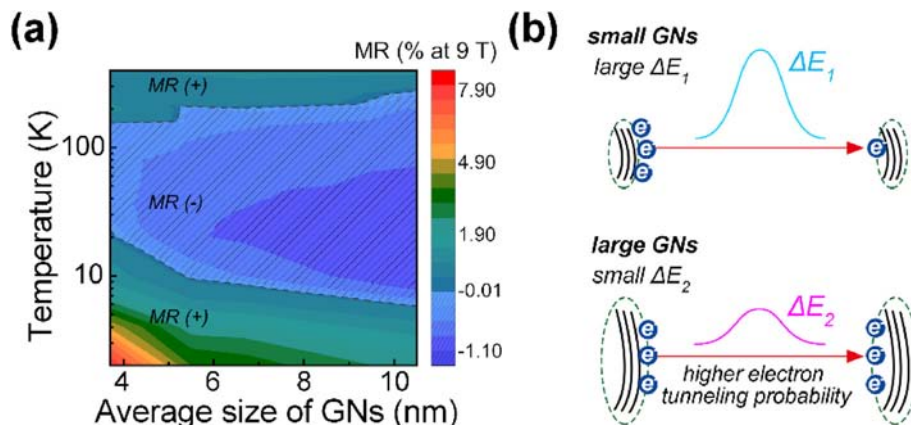


Fig. 6. (a) MR behavior as a function of temperature (from 2 K to 400 K) at 9 T for GNC films with various sizes of GNs; (b) schematic diagram of thermally activated electrons tunneling process as a consequence of spin-dependent Coulomb blockade effect for GNC films with small GNs and large GNs. (A colour version of this figure can be viewed online.)

while temperature increases up to ~ 160 K (GNC-3.7 nm), ~ 210 K (GNC-5.5 nm), ~ 210 K (GNC-6.7 nm) and ~ 300 K (GNC-10.5 nm). The origin of positive MR in this temperature range can be regarded as effect of Lorentz force (MR_{LF} (+)). Typically, at high magnetic field regime, MR_{Total} curves present non-saturating linear trend vs. B, as shown in Fig. S9. Under magnetic field at a higher temperature, the Lorentz force would curve path of carriers and result in an increased resistance eventually, this linear MR_{Total} vs. B was also previously observed in multilayer graphene [42,43].

Our experimental findings clearly demonstrate that GNC film exhibits temperature controllable magneto-transport properties. The MR behavior of GNC film can be synergistically tuned by the size of GNs and temperature, which provides important insights and guidance for targeted regulation to design sign adjustable and efficient magneto-electronic devices. Moreover, in our study, the carbon film consists of nano-sized magnetic GNs and amorphous carbon matrix. Since the electric conductivity of amorphous carbon matrix is much lower than GNs, the analogy of spin-related hopping mode was introduced to understand the origin and the crossover between $MR(+)$ and $MR(-)$, as well as its dependency on the GN sizes. From this work, we can so far establish a basic framework, not perfect but close enough, for a general start of truly understanding the MR behaviors of GNC film. Thinking further, there are other features might also have influences, such as the distance between GNs, stacking layer-to-in plane size ratio, or even the contribution from amorphous matrix. Further investigations are in demand to reveal the answers.

4. Conclusion

In this work, we observe two thermal driven sign changes of MR value from positive to negative and various magneto-transport behaviors in GNC films. We propose that the sign changes come from the competitions among different origins including wave function shrinkage, spin-dependent Coulomb blockade and Lorentz force, which play dominant roles in low, medium and high temperatures, respectively. At low temperature (2 K), MR_{Total} (+) are obtained from GNC films, the $\ln(\rho(B)/\rho(0))$ values of the films linearly increases with B^2 in low magnetic field, linearly increases with $B^{1/3}$ and presents saturated trend in strong magnetic field. Based on above fitting results, we propose the $MR(+)$ is derived from the effect of wave function shrinkage. As the temperature increases, the first transition from MR_{Total} (+) to MR_{Total} (-) appears. We infer from these results that the $MR(-)$ can be attributed to effect of spin-dependent Coulomb blockade effect. Moreover, it is

found that GNC film with larger GNs indicates larger $MR(-)$ value in a wide temperature range. This phenomenon is attributed to lower potential increase ΔE induced by large GN, resulting in higher electron tunneling probability. As the temperature further increases, the second transition from MR_{Total} (-) to MR_{Total} (+) is detected, which is unsaturated and linearly increased with B. The $MR(+)$ at high temperature can be regarded as effect of Lorentz force. This investigation shed light on the physical comprehension of electron transport property and MR behavior of graphene nanocrystalline based film, it also provided theoretical guidance for further design of spin electric devices with temperature-controlled MR signal, and expanded the application prospects of graphene derived materials in the field of magnetic sensors and magnetic logic devices.

Author contributions

C. Wang and D. Ding: conceived and designed the experiments. **C. Wang, D. Ding and X. Dai:** performed the experiments. **C. Wang, D. Diao and D. Ding:** co-wrote the paper. All authors discussed the results and commented on the manuscript. All authors have given approval to the final version of the manuscript.

Declaration of competing interest

The authors declare that they have no known competing financial interests or personal relationships that could have appeared to influence the work reported in this paper.

CRediT authorship contribution statement

Dong Ding: Conceptualization, Investigation, Validation, Data curation, Writing - original draft. **Xingze Dai:** Data curation. **Chao Wang:** Conceptualization, Investigation, Validation, Data curation, Resources, Supervision, Writing - original draft. **Dongfeng Diao:** Resources, Supervision, Writing - review & editing.

Acknowledgements

This work was funded by the National Natural Science Foundation of China (51875364), Project of Department of Education of Guangdong Province (No 2017KTSCX165), Guangdong Natural Science Foundation (2018A0303130086), Shenzhen Basic Research Layout Project (JCYJ20160427105015701), and Exploration Project (JCYJ20170302145418596). The authors would like to thank the

Electron Microscopy Center (EMC) of Shenzhen University for their technical supports in TEM and FIB.

Appendix A. Supplementary data

Supplementary data to this article can be found online at <https://doi.org/10.1016/j.carbon.2020.03.022>.

References

- [1] Z. Wang, X. Wang, M. Li, Y. Gao, Z. Hu, T. Nan, et al., Highly sensitive flexible magnetic sensor based on anisotropic magnetoresistance effect, *Adv. Mater.* 28 (2016) 9370–9377.
- [2] S. Albarakati, C. Tan, Z. Chen, J.G. Partridge, G. Zheng, L. Farrar, et al., Antisymmetric magnetoresistance in van der Waals $\text{Fe}_3\text{GeTe}_2/\text{graphite}/\text{Fe}_3\text{GeTe}_2$ trilayer heterostructures, *Sci. Adv.* 5 (2019), eaaw0409.
- [3] M. Rein, N. Richter, K. Parvez, X. Feng, H. Sachdev, M. Kläui, et al., Magnetoresistance and charge transport in graphene governed by nitrogen dopants, *ACS Nano* 9 (2) (2015) 1360–1366.
- [4] W. Wang, Y. Wang, L. Tu, T. Klein, Y. Feng, Q. Li, et al., Magnetic detection of mercuric ion using giant magnetoresistance based biosensing system, *Anal. Chem.* 86 (2014) 3712–3716.
- [5] Z. Luo, X. Zhang, C. Xiong, J. Chen, Silicon-based current-controlled reconfigurable magnetoresistance logic combined with non-volatile memory, *Adv. Funct. Mater.* 25 (2015) 158–166.
- [6] J. Sun, Y. Chen, M. Priyadarshi, Z. Chen, A. Bachmatiuk, Z. Zou, et al., Direct CVD-derived graphene glasses targeting wide ranged applications, *Nano Lett.* 15 (9) (2015) 5846–5854.
- [7] J. Bai, R. Cheng, F. Xiu, L. Liao, M. Wang, A. Shailos, et al., Very large magnetoresistance in graphene nanoribbons, *Nat. Nanotechnol.* 5 (2010) 655–659.
- [8] A.K. Singh, J. Eom, Negative magnetoresistance in a vertical single-layer graphene spin valve at room temperature, *ACS Appl. Mater. Interfaces* 6 (2014) 2493–2496.
- [9] J. Lu, H. Zhang, W. Shi, Z. Wang, Y. Zheng, T. Zhang, et al., Graphene magnetoresistance device in van der Pauw geometry, *Nano Lett.* 11 (2011) 2973–2977.
- [10] B.G. Shin, D.H. Boo, B. Song, S. Jeon, M. Kim, S. Park, et al., Single-crystalline monolayer graphene wafer on dielectric substrate of SiON without metal catalysts, *ACS Nano* 13 (2019) 6662–6669.
- [11] Y. Tang, L. Yin, Y. Yang, X. Bo, Y. Cao, H. Wang, et al., Tunable band gaps and p-type transport properties of boron-doped graphenes by controllable ion doping using reactive microwave plasma, *ACS Nano* 6 (3) (2012) 1970–1978.
- [12] H. Overweg, H. Eggimann, M. Liu, A. Varlet, M. Eich, P. Simonet, et al., Oscillating magnetoresistance in graphene p-n junctions at intermediate magnetic fields, *Nano Lett.* 17 (2017) 2852–2857.
- [13] Z. Yue, I. Levchenko, S. Kumar, D. Seo, X. Wang, S. Dou, et al., Large networks of vertical multi-layer graphenes with morphology-tunable magnetoresistance, *Nanoscale* 5 (2013) 9283–9288.
- [14] C.N.R. Rao, H.S.S. Ramakrishna Matte, K.S. Subrahmanyama, Urmimala Maitra, Unusual magnetic properties of graphene and related materials, *Chem. Sci.* 3 (2012) 45–52.
- [15] Z. Liao, H. Wu, S. Kumar, G.S. Duesberg, Y. Zhou, G.L.W. Cross, et al., Large magnetoresistance in few layer graphene stacks with current perpendicular to plane geometry, *Adv. Mater.* 24 (2012) 1862–1866.
- [16] X. Zhang, C. Wang, C. Sun, D. Diao, Magnetism induced by excess electrons trapped at diamagnetic edge-quantum well in multi-layer graphene, *Appl. Phys. Lett.* 105 (2014), 042402.
- [17] M. Zeb, B. Shabbir, R.U.R. Sagar, N. Mahmood, K. Chen, I. Qasim, M.I. Malik, et al., Superior magnetoresistance performance of hybrid graphene foam/metal sulfide nanocrystal devices, *ACS Appl. Mater. Interfaces* 11 (2019) 19397–19403.
- [18] W. Chen, Y. Zhou, S. Yu, W. Yin, C. Gong, Width-tuned magnetic order oscillation on zigzag edges of honeycomb nanoribbons, *Nano Lett.* 17 (2017) 4400–4404.
- [19] W.Y. Kim, K.S. Kim, Prediction of very large values of magnetoresistance in a graphene nanoribbon device, *Nat. Nanotechnol.* 3 (2008) 408–412.
- [20] Shyamal K. Saha, Moni Baskey, Dipanwita Majumdar, Graphene quantum sheets: a new material for spintronic applications, *Adv. Mater.* 22 (2010) 5531–5536.
- [21] M. Zeng, Y. Feng, G. Liang, Graphene-based spin caloritronics, *Nano Lett.* 11 (2011) 1369–1373.
- [22] L.A. Ponomarenko, F. Schedin, M.I. Katsnelson, R. Yang, E.W. Hill, K.S. Novoselov, et al., Chaotic Dirac billiard in graphene quantum dots, *Science* 320 (2008) 356–358.
- [23] S. Pisana, P.M. Braganca, E.E. Marinero, B.A. Gurney, Tunable nanoscale graphene magnetometers, *Nano Lett.* 10 (2010) 341–346.
- [24] R. Garg, D.P. Gopalan, S.C. de la Barrera, H. Hafiz, N.T. Nuhfer, V. Viswanathan, et al., Electron transport in multidimensional fuzzy graphene nanostructures, *Nano Lett.* 19 (2019) 5335–5339.
- [25] T. Reichert, G. Hagelestein, T.P.I. Saragi, Magnetic-field effects in ambipolar transistors based on a bipolar molecular glass, *Mater. Chem. Front.* 1 (2017) 1622–1628.
- [26] D. Ciudad, M. Gobbi, C.J. Kinane, M. Eich, J.S. Moodera, L.E. Hueso, Sign control of magnetoresistance through chemically engineered interfaces, *Adv. Mater.* 26 (2014) 7561–7567.
- [27] Y. Wang, X. Luo, L. Tseng, Z. Ao, T. Li, G. Xing, et al., Ferromagnetism and crossover of positive magnetoresistance to negative magnetoresistance in Nd-doped ZnO, *Chem. Mater.* 27 (2015) 1285–1291.
- [28] S.M. Wang, Y.H. Pei, X. Wang, H. Wang, Q.N. Meng, H.W. Tian, et al., Synthesis of graphene on a polycrystalline Co film by radio-frequency plasma-enhanced chemical vapour deposition, *J. Phys. D Appl. Phys.* 43 (2010) 455402.
- [29] A.C. Ferrari, D.M. Basko, Raman spectroscopy as a versatile tool for studying the properties of graphene, *Nat. Nanotechnol.* 8 (2013) 235–246.
- [30] C. Casiraghi, A. Hartschuh, H. Qian, S. Piscanec, C. Georgi, A. Fasoli, et al., Raman spectroscopy of graphene edges, *Nano Lett.* 9 (2009) 1433–1441.
- [31] D.V. Talapin, J. Lee, M.V. Kovalenko, E.V. Shevchenko, Prospects of colloidal nanocrystals for electronic and optoelectronic applications, *Chem. Rev.* 110 (2010) 389–458.
- [32] S. Lamba, D. Kumar, Variable-range hopping: role of coulomb interactions, *Phys. Rev. B* 59 (1999) 4752–4765.
- [33] Z. Luo, H. Piao, A.V. Brooks, X. Wang, J. Chen, C. Xiong, F. Yang, et al., Large magnetoresistance in silicon at room temperature induced by onsite coulomb interaction, *Adv. Electron. Mater.* 3 (2017) 1700186.
- [34] Y.Z. Long, Z.H. Yin, Z.J. Chen, Low-temperature magnetoresistance studies on composite films of conducting polymer and multiwalled carbon nanotubes, *J. Phys. Chem. C* 112 (2008) 11507–11512.
- [35] T. Su, C. Wang, S. Lin, R. Rosenbaum, Magnetoresistance of $\text{Al}_{70}\text{Pd}_{22.5}\text{Re}_{7.5}$ quasicrystals in the variable-range hopping regime, *Phys. Rev. B* 66 (2002), 054438.
- [36] A. Kurobe, H. Kamimura, Correlation effects on variable range hopping conduction and the magnetoresistance, *J. Phys. Soc. Jpn.* 51 (1982) 1904–1913.
- [37] A.G. Zabrodskii, The Coulomb gap: the view of an experimenter, *Phil. Mag. B* 81 (9) (2001) 1131–1151.
- [38] X.-G. Zhang, Z.C. Wen, H.X. Wei, X.F. Han, Giant coulomb blockade magnetoresistance in magnetic tunnel junctions with a granular layer, *Phys. Rev. B* 81 (2010), 155122.
- [39] Y. Wang, Z.Y. Lu, X.-G. Zhang, X.F. Han, First-principles theory of quantum well resonance in double barrier magnetic tunnel junctions, *Phys. Rev. Lett.* 97 (2006), 087210.
- [40] S.M. Thompson, The discovery, development and future of GMR: the Nobel Prize 2007, *J. Phys. Appl. Phys.* 41 (2008), 093001.
- [41] B. Abeles, P. Sheng, M.D. Coutts, Y. Arie, Structural and electrical properties of granular metal films, *Adv. Phys.* 24 (3) (1975) 407–461.
- [42] J. Chen, J. Meng, Y. Zhou, H. Wu, Y. Bie, Z. Liao, et al., Layer-by-layer assembly of vertically conducting graphene devices, *Nat. Commun.* 4 (2013) 1921.
- [43] A.L. Friedman, J.L. Tedesco, P.M. Campbell, J.C. Culbertson, E. Aifer, F.K. Perkins, et al., Quantum linear magnetoresistance in multilayer epitaxial graphene, *Nano Lett.* 10 (2010) 3962–3965.